inter.noise
HAMBURG 2016

Free-Field Pressure-Based Sound Power Measurement Procedure with Low Spatial-Sampling- and Near-Field-Induced Uncertainty

Hannes Pomberger[1]; Franz Zotter[1]; Alois Sontacchi[1]; Manuel Brandner[1];
Markus Resch[2]; Stephan Brandl[2]; Robert Höldrich[1]
[1]Institut für Elektronische Musik und Akustik,
Universität für Musik und Darstellende Kunst, Graz, Austria
[2]AVL LIST GmbH, Austria

ABSTRACT

Undoubtedly, engine sound power is a well-suited benchmark that characterizes the over-all sound emission of, e.g., combustion engines in vehicles. A grade-1 standard procedure specifies a way to determine sound power by simultaneous measurement using 20 microphones spherically surrounding the engine within an anechoic chamber. In this contribution, we improve the achievable accuracy by utilizing a grid of only 16 microphones that provides more accurate sampling and more accurate estimation, in particular in combination with the consideration of acoustical near-fields.

In a theoretical study we can demonstrate the improved accuracy based on (i) rotation statistics of simulated engine measurement data, (ii) a diffuse spherical model, and (iii) a directional spherical model of a velocity source. In all the three cases, the sound power is exactly known, which permits an accurate analysis of emerging uncertainties. From practical testbed measurements, we can validate the proposed grade-1 procedure by demonstrating the preservation of basic statistical relationships found in theoretical considerations. Finally, this article discusses measures obtained by analyzing the 16 microphone signals, suitable to indicate the frequency range in which a grade-1 accuracy can be expected.

Keywords: Sound Power, Near-Field, Spatial Sampling
I-INCE Classification of Subjects Number(s): 77, 72.4

1. INTRODUCTION

Sound power measurement procedures are designed for high reproducibility. Standards specify tolerances for acoustic environments, equipment, and also layouts for the microphone positions. As one of the grade 1 (precision) methods for sound power measurement, the ISO 3745 [1] proposes to use a grid of $\mathrm{M} = 20$ (if necessary 40) points on a sphere for simultaneous measurements in an anechoic room. The idea of the proposed grid is to achieve equal-area coverage. Far field conditions are assumed to be met when the radius R of the measurement array is at least a fourth wave length, one meter, and twice the largest source diameter. At one frequency, the sound power is estimated from the spatial sound pressure samples p_i

$$\hat{\Pi} = \frac{1}{2}\,\frac{1}{\rho c}\,\frac{4\pi \mathrm{R}^2}{\mathrm{M}} \sum_{i=1}^{\mathrm{M}} |p_i|^2, \tag{1}$$

where c is the speed of sound and ρ is the density of air. The equation text in the norm is just differently formulated as it requires dB values and gathers constants, corrections, and normalizations. The expression is a discretized version of the analytic far-field sound power $\Pi = \frac{1}{2}\,\frac{1}{\rho c} \oint_S |p|^2 \,\mathrm{d}S$ using the average surface element $\frac{4\pi \mathrm{R}^2}{\mathrm{M}}$. The far-field sound power relates to the definition of sound power $\Pi = \frac{1}{2} \oint_S \Re\{p\,\boldsymbol{v}^*\} \cdot \mathrm{d}\boldsymbol{S}$ by acknowledging that the particle velocity $\boldsymbol{v}$ is strictly aligned with the outward normal and proportional to the sound pressure $v = \frac{p}{\rho c}$ in the far field.

[1]email: pomberger@iem.at

Even under perfect measurement conditions (perfectly calibrated and placed microphones, perfectly anechoic room), estimation according to the discretized far-field sound-power integral of Eq. (1) inherits two intrinsic sources of estimation uncertainty:

- violation of the far field assumption at low frequencies,
- effects of the spatial discretization (sampling grid and its orientation).

Even if it is not generally possible to avoid above-mentioned uncertainties, a drastic reduction of uncertainty stemming from near-fields and spatial sampling has been demonstrated in [2]. In this recent work, we reduced uncertainties by proposing an alternative 16-points spherical sampling grid and involved near fields in the estimation to avoid the typical, systematic sound power over estimation at low frequencies. The study of the improvements was based on the sound field radiated by a simulated car engine. Still, the proposed measurement technique used a measurement radius of R=1.4 m, and the 16-points grid nearly appears irregular to set up, angularly.

In the present paper, first the near-field involving estimator is recapitulated, and the achievable accuracy for a more practical measurement is discussed with a smaller measurement radius R=75 cm. The new proposition is to arrange the 16 points in three rings and one measurement point at the zenith, as given in Table 1. The condition number $\kappa = 2.09$ for spherical harmonics decomposition with the new 16-points grid is only slightly worse than the condition number $\kappa = 1.55$ of the originally proposed grid in [2], which is acceptable considering the practical advantages. The analysis of uncertainty in this paper is extended by two types of artificial sources, and a practical application is given, for which it is desirable to estimate the high-frequency boundary of accuracy from the measured data.

Table 1: Proposed practical spherical sampling grid of 16 points in 4 height levels (given in azimuth ϕ and zenith angle θ).

pos.	1	2	3	4	5	6	7	8	9	10	11	12	13	14	15	16
ϕ	0°	20°	100°	140°	220°	260°	340°	0°	60°	120°	180°	240°	300°	60°	180°	300°
θ	0°	60°	60°	60°	60°	60°	60°	110°	110°	110°	110°	110°	110°	150°	150°	150°

2. COMPOSITE NEAR-FIELD-INVOLVING SOUND POWER ESTIMATOR

In [2] we proposed to use a composite sound power estimator

$$\hat{\Pi} = \frac{1}{2\rho c}\min\left\{\frac{4\pi \mathrm{R}^2}{\mathrm{M}}\sum_{i=1}^{\mathrm{M}}|p_i|^2, \sum_{n,m}\frac{|\hat{\psi}_{nm}|^2}{k^2|h_n(k\mathrm{R})|^2}\right\} \tag{2}$$

where $\hat{\psi}_{nm}$ are the estimated coefficients of the sound pressure expanded in spherical harmonics, $h_n(kR)$ are the spherical Hankel functions of the second kind, and $k = \omega/c$ is the wave number. This estimator is able to avoid near-field induced over-estimation at low frequencies by its right-hand argument (see appendix). The argument on the left is the original discretized far-field sound power estimator, which is more accurate at high frequencies, where the other estimator has a slight (0.3 dB) systematic over-estimation tendency related to the condition number $\kappa \neq 1$ for the spherical harmonics decomposition that obtains $\{\hat{\psi}_{nm}\}$ from $\{p_i\}$.

Using a well-distributed spherical measurement grid defined by a set of Cartesian unit vectors $\{\boldsymbol{\Theta}_i\}$, the sound pressure samples $\boldsymbol{p} = [p(\boldsymbol{\Theta}_i)]_{i=1\ldots\mathrm{M}}$ can be expanded into a linear combination of spherical harmonics $p = \sum_{n,m}\psi_{nm}Y_n^m(\boldsymbol{\theta})$ using the unknown coefficients ψ_{nm}. To find the coefficients, the sampled spherical harmonics up to the orders $0 \leq n \leq \mathrm{N}$ are written into a matrix $\boldsymbol{Y}_\mathrm{N} = [Y_n^m(\boldsymbol{\Theta}_i)]_{i=1\ldots\mathrm{M}}^{n=0\ldots\mathrm{N},|m|\leq n}$, as well as the coefficients $\boldsymbol{\psi}_\mathrm{N} = [\psi_{nm}]_{n=0\ldots\mathrm{N},|m|\leq n}$. The best fitting $\boldsymbol{p}_\mathrm{N} = \boldsymbol{Y}_\mathrm{N}\,\boldsymbol{\psi}_\mathrm{N}$ estimate is then obtained by

$$\hat{\boldsymbol{\psi}}_\mathrm{N} = \left(\boldsymbol{Y}_\mathrm{N}^\mathrm{T}\boldsymbol{Y}_\mathrm{N}\right)^{-1}\boldsymbol{Y}_\mathrm{N}^\mathrm{T}\,\boldsymbol{p}. \tag{3}$$

To enable inversion, the sampling grid must contain at least $\mathrm{M} \geq (\mathrm{N}+1)^2$ measurement positions that provide a reasonable low condition number of $\boldsymbol{Y}_\mathrm{N}$. Inversion is ill-conditioned using the grid proposed in the ISO 3745 [1]. Moreover, we could show in [2] that the number of sampling points must equal the number of

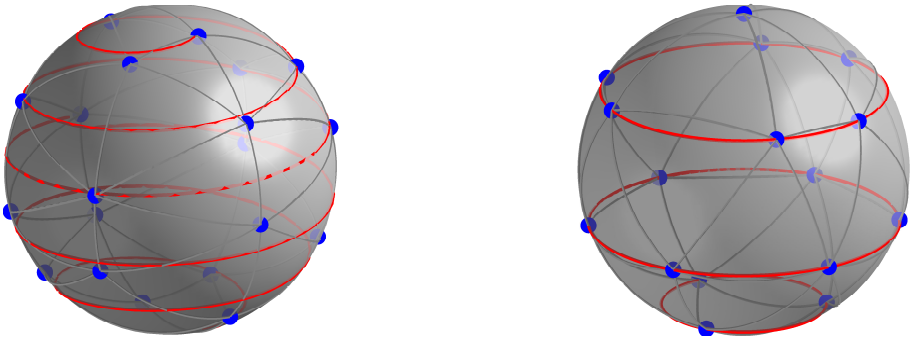

(a) 20pt. measurement grid from ISO 3745 [1]

(b) proposed 16pt. measurement grid

Figure 1: Sampling scheme.

estimated spherical harmonic coefficients to avoid under-estimation at high frequencies. An optimal grid of 16 minimum determinant points [3] was suggested. A new arrangement of 16 points is proposed here (Tab. 1), which is more practically arranged in horizontal rings, Fig. 1b.

3. THEORETICAL STUDY

This section discusses the accuracy of the different sound power estimators and grids at a measurement radius of R=75 cm with the formulation of a 19^{th}-order continuous sound pressure distribution as a starting point:

$$p(k\mathrm{R}, \boldsymbol{\theta}) = \sum_{n=0}^{19} \sum_{m=-n}^{n} \psi_{nm}(k\mathrm{R})\, Y_n^m(\boldsymbol{\theta}), \tag{4}$$

whose exact sound power (ground truth) is known to be, see also [4],

$$\Pi = \frac{1}{2}\,\frac{1}{\rho\, c}\,\frac{1}{k^2} \sum_{n,m} \frac{|\psi_{nm}|^2}{|h_n(k\mathrm{R})|^2}. \tag{5}$$

For the simulation study, the continuous sound pressure distribution of Eq. (4) is sampled on the spherical measurement grid $\{\vartheta_i\}$ to obtain the discrete sound pressure values $p_i = p(\vartheta_i)$ required by the estimators Eqs. (2,3) and Eq. (1).

Obviously, the orientation of the measurement grid relative to the source does not change the radiated power. However, the estimated sound power might vary for different relative orientations. As the relative orientation is arbitrary, we propose to use this variation to quantify the uncertainty caused by the measurement grid. Using J uniformly distributed random rotations of a unit sphere, see [5, p. 117], in terms of rotation matrices $\boldsymbol{R}_j$, a set of sound power estimations $\{\hat{\Pi}_1, \ldots \hat{\Pi}_j, \ldots \hat{\Pi}_\mathrm{J}\}$ is achieved by applying the random rotations to the measurement grid $\{\boldsymbol{R}_j\, \vartheta_i\}$ prior to discretization. The deviation from the ground-truth value in dB is calculated by $\Delta L_{\mathrm{w,j}} = 10\log_{10}(\Pi) - 10\log_{10}(\hat{\Pi}_j)$.

Simulated engine data: This study uses a simulated engine data obtained from the AVL Excite[3] environment. The sound pressure emitted by the simulated engine defines $\psi_{nm}(k\mathrm{R})$ at R=75 cm. The simulation yields values $\psi_{nm}(k\mathrm{R})$ for integer multiples $f_l = l\, f_0$ of a fundamental frequency f_0.

To improve readability of the sparse engine sound power spectra, the resulting estimators $\hat{\Pi}_j$ were octave smoothed. To gather sound power values $\Pi(f_l)$ available at the bins l, a Hann window was employed. The particular estimation of the octave-smoothed value around the center frequency f_c is obtained by the sum of bin values $\Pi(f_l)$ times the average of the Hann window across the each bin interval $f \in [f_l - f_0/2;\, f_l + f_0/2]$

$$\Pi(f_c) = \sum_l \Pi(f_l)\, \frac{1}{f_0} \int_{-f_0/2}^{f_0/2} \cos^2\!\left(\tfrac{\pi}{2}\, \min\{|\log_2(f_l + f) - \log_2(f_c)|, 1\}\right) \mathrm{d}f. \tag{6}$$

The estimation uncertainty according to ISO 3745 [1] with $\mathrm{M} = 20$, cf. Fig. 1a, and Eq. (1) is shown in Figs. 2(a) to (d). The deviation ΔL_W of the sound power estimators $\hat{\Pi}$ from the ground truth Π was analyzed

[3] http://www.avl.com/web/ast/excite

with the above-proposed rotation statistics using 1000 random rotations. The median value of ΔL_{W} is shown as solid curve, the 50% inter-quartile range as dark-gray area, and the 95% inter-quartile range as light-gray area. The results show the typical over estimation at low frequencies due to near fields; the step-shaped contours at higher rpm numbers (3000, 4000) are merely due to the sparse appearance of the lowest spectral component at (50, 67) Hz.

Using the composite, near-field-involving estimator Eqs. (2,3) and the 16 point grid from Tab. 1 / Fig. 1b yields the rotation statistics shown in Figs. 2 (e) to (g). The composite estimator does not exhibit systematic over estimation at low frequencies and minimizes the statistical spread at most frequencies.

In the analysis of our previous paper [2], the near-field effects were less drastic, as a larger measurement radius R=1.4 m was simulated. Obviously, the near-field-involving estimator is suitable to obtain accurate results for much smaller measurement setups. This is of practical relevance for testbed setups, in which engines are typically attached to the testbed at a height of about 85cm, and larger setups would need to extend below the floor.

3.1 Directional spherical cap radiator model

The above study deals with one simulated engine in four different rpm conditions. To obtain a less specific and maybe more general insight about what sound power estimation does, an artificial radiator is introduced that should produce worst-case results, in particular at high frequencies. This is achieved by modeling a vibrating spherical cap of unit velocity. The spherical harmonics expansion of a velocity pattern on a sphere is expressed by the boundary condition

$$v_r(\boldsymbol{\theta}) = \sum_{n=0}^{\infty} \sum_{-m}^{m} \gamma_{nm} Y_n^m(\boldsymbol{\theta}). \tag{7}$$

For a spherical cap, the coefficients γ_{nm} for sound particle velocity become

$$\gamma_{nm} = Y_n^m(\boldsymbol{\theta}_c)\, w_n(\alpha), \tag{8}$$

where $\boldsymbol{\theta}_c$ is the direction of the cap center, and $\alpha_n(\alpha)$ is the order weight depending on the opening angle of the spherical cap α,

$$w_n(\alpha) = \begin{cases} P_{n-1}(\cos(\frac{\alpha}{2})) - \cos(\frac{\alpha}{2}) P_n(\cos(\frac{\alpha}{2})), & n > 0, \\ 1 - \cos(\frac{\alpha}{2}), & n = 0. \end{cases} \tag{9}$$

Assuming the spherical cap radiator's surface at the radius $r = a$, we obtain the coefficients $\psi_{nm}(k\mathrm{R})$ at the radius R as, cf. [4]

$$\psi_{nm}(k\mathrm{R}) = \frac{\rho_0 c\; h_n(k\mathrm{R})}{\mathrm{i}\, h_n'(ka)}\, \gamma_{nm}. \tag{10}$$

In the simulation study for a spherical cap radiator, with $\alpha = 14^\circ$ and $a = 0.4$ m, the direction $\boldsymbol{\theta}_c$ is randomly varied in 1000 instances (rotation statistics). Fig. 3 shows the statistics revealing the sound power uncertainty for both estimators. As before, the solid line marks the median value, the dark-gray area marks the 50% inter-quartile range, and the light-gray area marks the 95% inter-quartile range.

For the ISO estimator in Fig. 3a, an over-estimation bias of about 1 dB is found at low frequencies, and the uncertainty at low frequencies is not as narrow as it could be, cf. Fig. 3b. The low-frequency near-field-induced over estimation for the ISO estimator is not as large as with the simulated engine. This follows a simple explanation: the spherical cap radiator *always* contains a 0^{th} order component (omnidirectional), which dominates the radiated sound power at low frequencies.

While the composite estimator reduces the statistical spread at frequencies below 300 Hz, around 300 to 500 Hz there seems to be a transition effect yielding larger (but more symmetrical) spread for the composite estimator, cf. Fig. 3b. At larger frequencies, both estimators behave similarly.

Generally, the spherical cap radiator poses a worst case to high-frequency sound power estimation: As soon as the main lobe of its directional sound radiation fits between the measurement positions, the estimator is prone to severe under estimation of sound power. At the same time, whenever one of the measurement positions lies on the main lobe of radiation, sound power gets largely over estimated. Both effects yield an increased spread and a bias towards a statistically more likely under estimation of sound power.

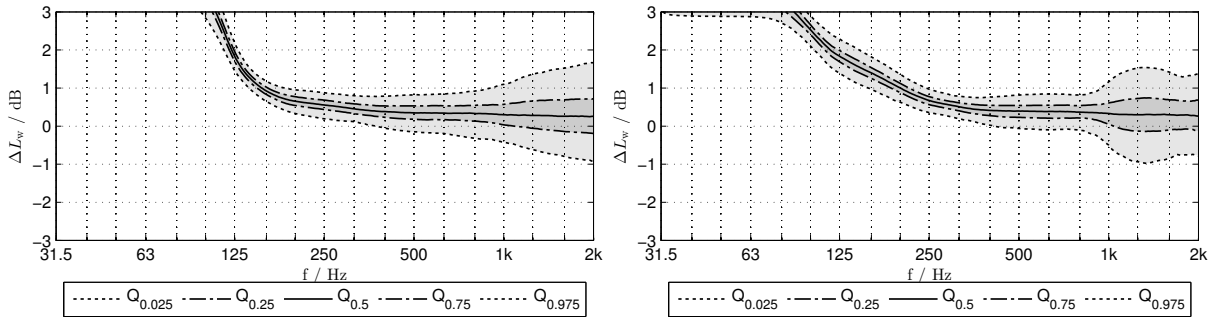

(a) rpm 1000

(b) rpm 2000

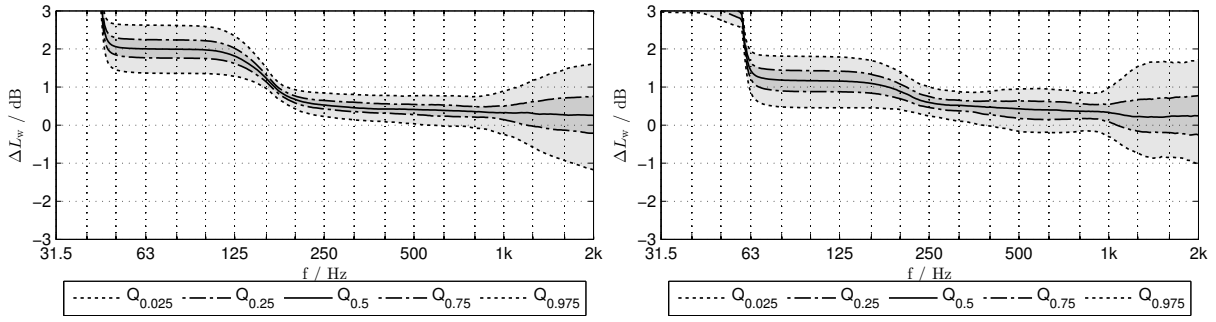

(c) rpm 3000

(d) rpm 4000

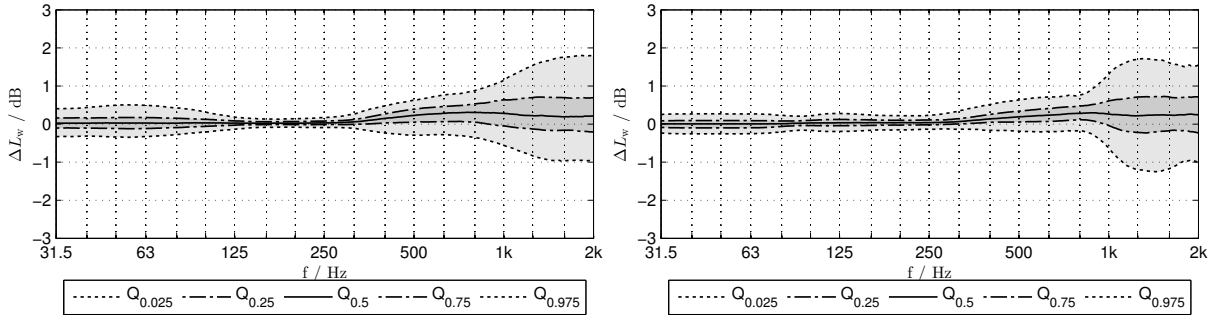

(e) rpm 1000

(f) rpm 2000

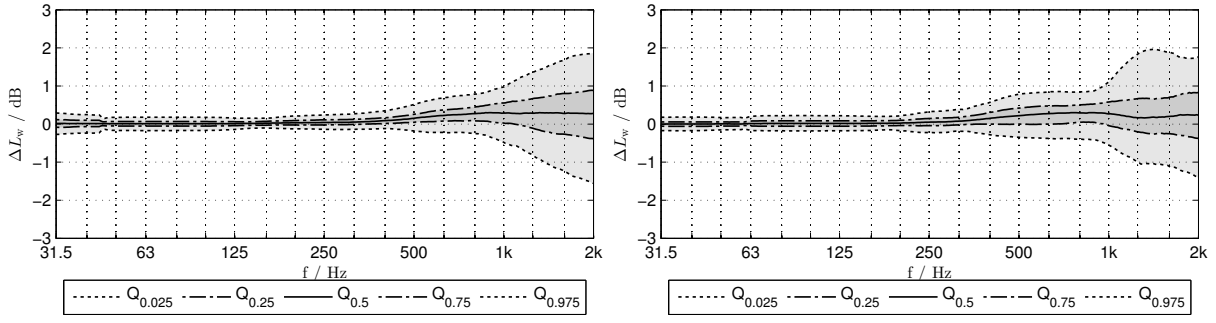

(g) rpm 3000

(h) rpm 4000

Figure 2: Rotational statistics of sound power estimator uncertainty for simulated engine measurement data for different rpm using the $\mathrm{M} = 20$ points estimator Fig. 1a / Eq. (1) from the ISO 3745 [1] shown in (a) to (d) and the $\mathrm{M} = 16$ grid from Tab. 1 / Fig. 1b using the estimator [2] in Eqs. (2,3) for (e) to (h).

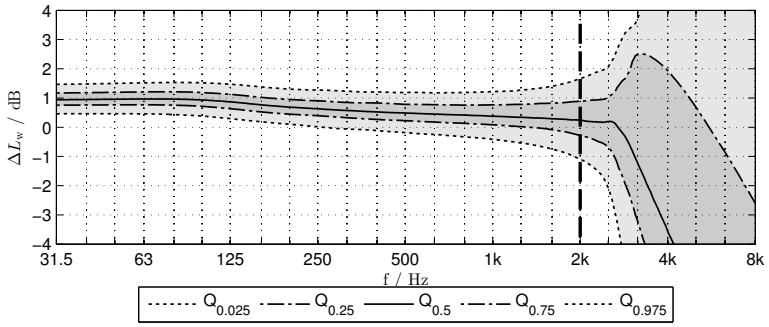

(a) $\mathrm{M} = 20$ points estimator Fig. 1a/Eq. (1) from the ISO 3745 [1]

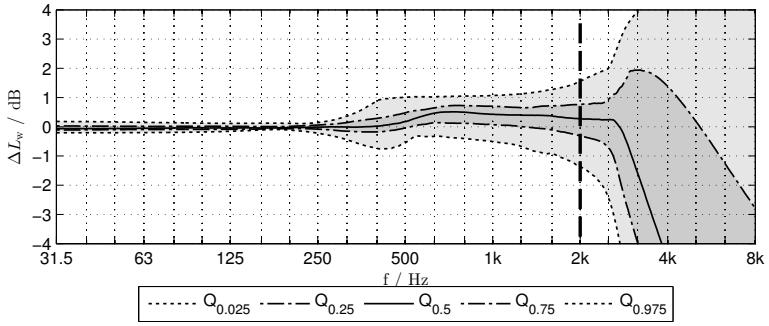

(b) $\mathrm{M} = 16$ grid from Tab. 1/Fig. 1b using the estimator [2] in Eqs. (2,3)

Figure 3: Rotational statistics of the sound power estimation uncertainty using the simulated cap model radiator and the different estimators.

3.2 Diffuse spherical radiator model

As opposed to the directional spherical cap radiator model described in the previous subsection, we assume a diffuse spherical radiator with random-velocity boundary condition. The spatially normally distributed random velocity pattern on the surface of such a radiator transforms to normally distributed expansion coefficients γ_{nm} to be inserted in Eq. (10).

In the simulation study for the diffuse radiator, 1000 coefficients sets of γ_{nm} were randomly generated to cover sufficiently much variation in the random process for the statistics on deviations of sound power estimators. An additional rotation statistics of these 1000 random coefficient sets can be omitted: Random rotations of random patterns are also random.

Fig. 4 shows the deviation statistics of both the sound power estimators. The diffuse radiator exhibits the typical near-field-induced over estimation at low frequencies when using the ISO estimator in Fig. 4a. The average over estimation can be less than with the engine simulation in Fig. 2 (a) to (d), but the uncertainty is much larger due to the random composition of the spherical harmonic components. For the diffuse radiation model, the composite estimator removes the over estimation and yields a negligible uncertainty at low frequencies, see Fig. 4b.

Note that with the estimator of Eq. (1), the only case where near-fields are entirely absent is when the zeroth-order component γ_{00} is dominant. As this is a seldom limit case of the random process, the sound power at low frequencies can only be over estimated in Fig. 4a.

Closer inspection of Figs. 4a and 4b reveals that the high-frequency sound power uncertainty remains constant for the diffuse radiator after a certain frequency (1 kHz). Above this limit, the number of observable degrees of freedom of the random process is limited by the number of measurement points. Hence, the $\mathrm{M} = 20$ grid has a slight, but negligible, advantage at higher frequencies when compared to estimation with $\mathrm{M} = 16$ points: the larger number of points yields a reduced statistical spread.

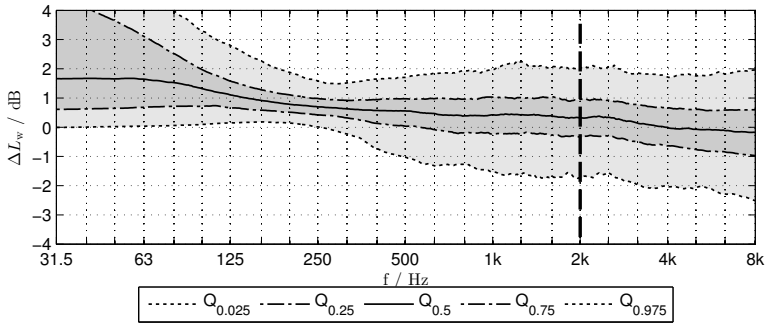

(a) M = 20 points estimator Fig. 1a / Eq. (1) from the ISO 3745 [1]

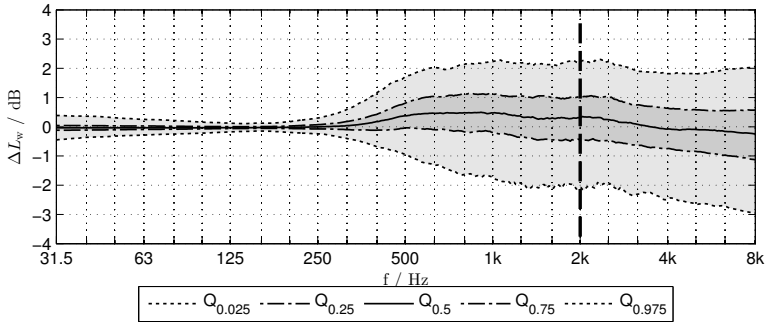

(b) M = 16 grid from Tab. 1 / Fig. 1b using the estimator [2] in Eqs. (2,3)

Figure 4: Statistics of the sound power estimation uncertainty using a stochastically diffuse radiator model and the different estimators.

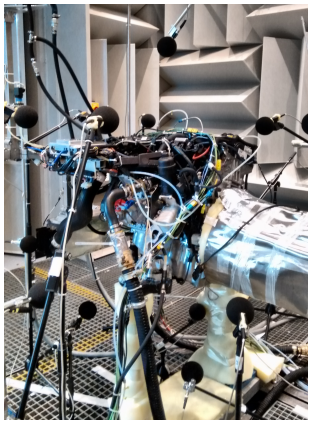

(a) Testbed measurement setup.

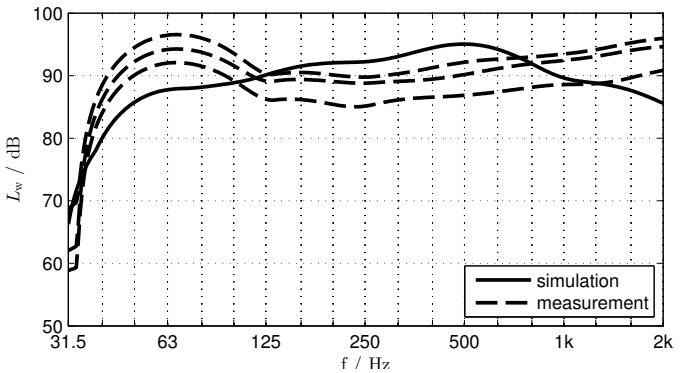

(b) Measured sound power for 0%, 50%, 100% loads compared to simulated engine at 2000 rpm. Note that the lower frequency limit of the testbed is about 125 Hz; the peak arround 63Hz is due to the room.

Figure 5: Sound power estimation using the proposed 16-points measurement grid and the composite estimator in practice.

4. TESTBED MEASUREMENTS

On September 9$^{\text{th}}$ in 2015, a combustion engine depicted in Fig. 5a was measured in AVL's larger engine testbed to apply the new 16-points measurement grid in Tab. 1 and the estimator in Eqs. (2,3) in practice.

Fig. 5 compares the measured sound power using the proposed grid and estimator in comparison to the sound power from the simulated engine of theoretical study about uncertainty with 2000rpm. The measured and simulated sound power spectrum are obviously not the same. However, the simulated engine is not the same as the one used for the testbed measurements and thus the engines might not only differ in their sound power spectrum but also might have different radiation patterns as well. Therefore the question of how accurately the sound power is estimated in the practical testbed measurement is difficult to answer.

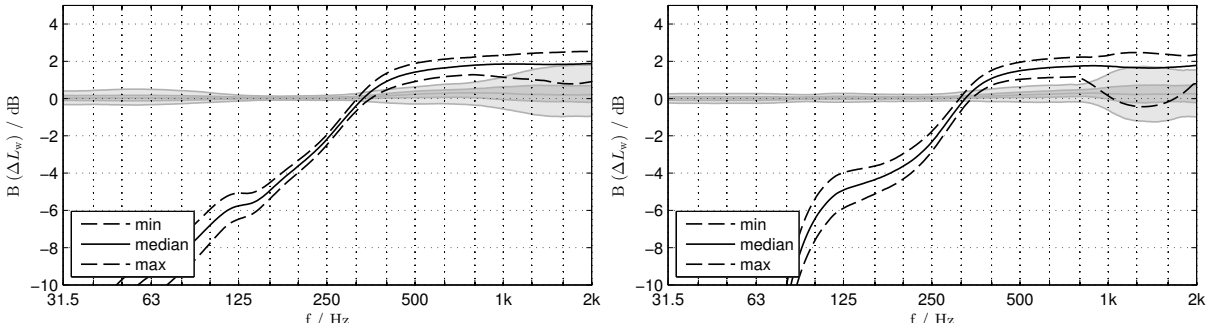

(a) rpm 1000

(b) rpm 2000

(c) rpm 3000

(d) rpm 4000

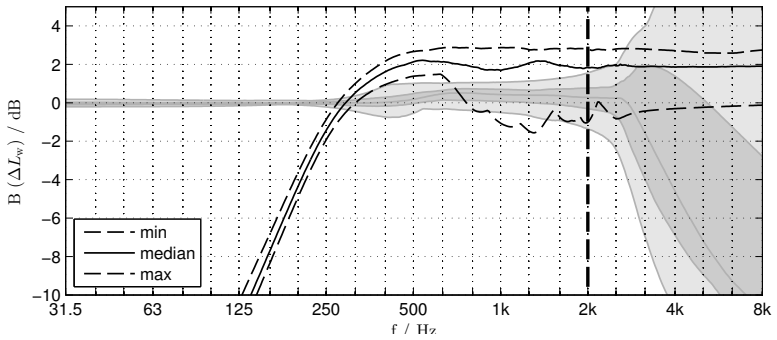

(e) rpm 4000

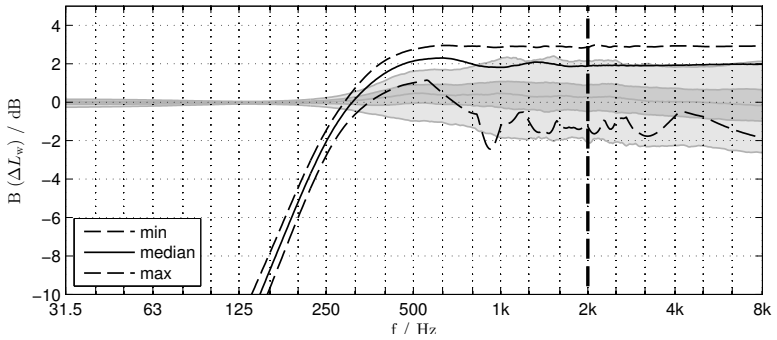

(f) rpm 4000

Figure 6: Rotation statistics of low- to all-order energy ratio $B(f)$ compared to statistical spread for different engine speeds (a) to (d), and the analysis for the spherical cap radiator model (e) and diffuse radiator model (f)

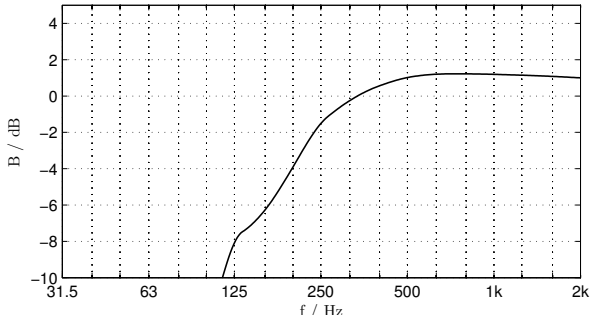

Figure 7: Rotation statistics of low- to all-order energy ratio $B(f)$ for the testbed measurement.

Estimation of upper frequency limits: Nevertheless, some similarity comparisons and parallels can be made between measures and statistical inter-quartile ranges of all simulated radiators, if there is a reasonable way to define crucial measures of describing where uncertainty begins.

As a key point in this endeavor, we observe that the composite, near-field-involving estimator mainly exhibits a statistical spread in sound power estimation that increases with frequency for all types of radiators used in the analysis about the statistical estimation uncertainty, see Figs. 2 (e) to (g), Fig. 3b, and Fig. 4b.

Thus it is a plausible assumption that for any radiator of finite size and complexity, the acoustic radiation efficiency of higher-order spherical harmonics components increases with frequency and becomes responsible for the increase in statistical spread. To capture this behavior, the ratio of low- to all-order energy of the estimated spherical harmonic coefficients $\hat{\psi}_{nm}$ is taken as a characteristic measure

$$B(f) = 2\frac{\sum_{n=0}^{1}\sum_{m=-n}^{n}|\hat{\psi}_{nm}|^2}{\sum_{n=0}^{3}\sum_{m=-n}^{n}|\hat{\psi}_{nm}|^2}. \tag{11}$$

Figs. 6 shows minimum, maximum, and median of $B(f)$ for the radiators of the theoretical study, calculated for random grid rotations. For the diffuse radiator model a single random coefficient set was employed to focus the investigation of interdependencies between $B(f)$ and ΔL_{w} to a single instance of a source.

For the simulated engine, Figs. 6 (a) to (d) illustrate that the transition of the measure from $B(f) < 1$ to $B(f) > 1$ is nicely able to predict the upper frequency limit for the simulated engine, above which the spread of the sound power estimation uncertainty increases. For the spherical cap radiator model in Fig. 6 (e) and the diffuse radiator model in Fig. 6 (f), the transition of $B(f)$ through a ratio of 1 is similar up to 600 Hz. For higher frequencies the minimum of the estimator is not as monotonic as for the engine simulation. In this frequency the estimator is not meaningful, as components with spherical harmonics order > 3 are aliased into the estimated $\hat{\psi}_{nm}$, $n \leq 3$.

Fig. 7 shows the ratio of low- and all-order spherical harmonic coefficients $B(f)$ for the testbed measurement. It shows a very similar characteristic to the simulated engine data. Hence we assume that the $B(f) < 1$ to $B(f) > 1$ transition is a plausible indicator for the upper frequency limit for accurate sound power estimation. As all modeled radiators exhibit rather similar uncertainty, at least up to 2 kHz, one can expect a similar increase of uncertainty for the practical testbed measurement.

5. CONCLUSION

In this contribution we reviewed a composite near-field-involving sound power estimator presented in [2] that is able to strongly suppress over estimation at low frequencies and leads to a more accurate and practical measurement procedure, especially if the sensors are not in the far-field of the radiating source. We showed the statistical uncertainties of the estimator for several types of sources (simulated combustion engine, simulated spherical cap radiator, simulated diffuse spherical radiator) in a measurement setup of 16 microphones in horizontal rings and at a radius of only $\mathrm{R} = 75$ cm and compared it to the 20 microphone setup proposed in the ISO 3745 [1].

Moreover, the application in practice was shown based on a testbed measurement of a combustion engine, for which no ground truth is accessible in most cases. Still, we managed to demonstrate the ratio of spherical-harmonic coefficient energies as plausible measure indicating the upper frequency limits of the estimation procedure.

6. ACKNOWLEDGMENT

We thank the Advanced Simulation Technology department of AVL GmbH, Günter Offner and Achim Hepberger, for making available simulated engine data to us. This work was supported by the project ASD, which is funded by Austrian ministries BMVIT, BMWFJ, the Styrian Business Promotion Agency (SFG), and the departments 3 and 14 of the Styrian Government. The Austrian Research Promotion Agency (FFG) conducted the funding under the Competence Centers for Excellent Technologies (COMET, K-Project), a program of the above-mentioned institutions.

REFERENCES

[1] ISO 3745: Acoustics — Determination of sound power levels and sound energy levels of noise sources using sound pressure — Precision methods for anechoic rooms and hemi-anechoic rooms, 2012.

[2] Hannes Pomberger, Franz Zotter, Robert Höldrich, and Stephan Brandl. Estimating errors in pressure-based engine sound power measurement due to spatial sampling. In *Proc. Congress Alps Adria Acoust. Assoc., Graz*, 2014.

[3] R. S. Womersley and I. H. Sloan. How good can polynomial interpolation on the sphere be? *Advances in Computational Mathematics*, 14, 2001.

[4] Earl G. Williams. *Fourier Acoustics*. Academic Press, 1999.

[5] D. Kirk. *Graphic Gems III*. Academic Press, 1995.

A. NEAR-FIELD-INVOLVING ESTIMATOR

According to Williams [4], the sound pressure on the surface of a sphere of radius r due to an arbitrary source within sphere is expressed by

$$p = \sum_{n=0}^{\infty} \sum_{m=-n}^{n} c_{nm}(k)\, h_n(kr)\, Y_n^m(\boldsymbol{\theta}), \tag{12}$$

where $h_n(kr)$ are the spherical Hankel functions of the second kind, $Y_n^m(\boldsymbol{\theta})$ are the spherical harmonics, $k = \omega/c$ is the wave number, and the coefficients $c_{nm}(k)$ are the wave spectrum of the source. The radiated sound power of the source is determined by the wave spectrum, cf.[4]

$$\Pi = \frac{1}{2}\,\frac{1}{\rho\, c}\,\frac{1}{k^2} \sum_{n,m} |c_{nm}(k)|^2. \tag{13}$$

If we had a spherical harmonics expanded sound pressure ψ_{nm} at $r = \mathrm{R}$, we would obtain a sound power estimate

$$\Pi = \frac{1}{2}\,\frac{1}{\rho\, c}\,\frac{1}{k^2} \sum_{n,m} \frac{|\psi_{nm}|^2}{|h_n(k\mathrm{R})|^2} \tag{14}$$

through $c_{nm} = \frac{\psi_{nm}}{h_n(k\mathrm{R})}$ that takes near field components into account, which appear for higher than zeroth order.